A microtubule-dependent zone of active RhoA during cleavage plane specification

William M. Bement,[1,2] Hélène A. Benink,[2] and George von Dassow[1]

[1]Center for Cell Dynamics, Friday Harbor Laboratories, University of Washington, Friday Harbor, WA 98250
[2]Department of Zoology, University of Wisconsin-Madison, Madison, WI 53706

THE JOURNAL OF CELL BIOLOGY

Cytokinesis in animal cells results from the assembly and constriction of a circumferential array of actin filaments and myosin-2. Microtubules of the mitotic apparatus determine the position at which the cytokinetic actomyosin array forms, but the molecular mechanisms by which they do so remain unknown. The small GTPase RhoA has previously been implicated in cytokinesis. Using four-dimensional microscopy and a probe for active RhoA, we show that active RhoA concentrates in a precisely bounded zone before cytokinesis and is independent of actin assembly. Cytokinetic RhoA activity zones are common to four echinoderm species, the vertebrate *Xenopus laevis,* and the highly asymmetric cytokinesis accompanying meiosis. Microtubules direct the formation and placement of the RhoA activity zone, and the zone is repositioned after physical spindle displacement. We conclude that microtubules specify the cytokinetic apparatus via a dynamic zone of local RhoA activity.

Introduction

In animal cells, cytokinesis is accomplished by an array of actin filaments and myosin-2 that assembles and closes at the cell equator between the separating chromosomes. Nearly 50 yr ago, it was demonstrated that physical extirpation of the mitotic spindle prevents formation of the cytokinetic apparatus in echinoderm embryos (Hiramoto, 1956). In the years since then, a variety of physical (Rappaport and Conrad, 1963), pharmacological (Hamaguchi, 1975), and molecular genetic (Abraham et al., 1983) approaches have confirmed that microtubules direct cytokinetic array assembly and positioning and do so via a mechanism that is remarkably plastic. That is, the signal provided by microtubules for cytokinetic apparatus specification is operative during an incredibly broad range of biological variation, including equilateral, unilateral, and asymmetric cytokinesis, and spans several orders of magnitude in cell size (Rappaport, 1996). It is also operative in the face of experimental manipulations that drastically change the relationship between the spindle and cell surface (Rappaport, 1961; Alsop and Zhang, 2004). This plasticity befits the importance of cytokinesis. At present, however, the signal(s) provided by microtubules that direct cytokinetic apparatus specification remains mysterious, as does the basis of its plasticity.

RhoA is a small GTPase that positively regulates actomyosin contractility. Based on studies using RhoA inhibitors or molecular genetic manipulation, RhoA is thought to be required for cytokinesis in diverse organisms (Kishi et al., 1993; Mabuchi et al., 1993; Drechsel et al., 1997; Jantsch-Plunger et al., 2000). Furthermore, RhoA localizes to the furrow region in mammalian cells (Takaishi et al., 1995; Yonemura et al., 2004). In addition, Ect2 (also known as Pbl), a RhoA guanine nucleotide exchange factor that promotes RhoA activation, localizes to the cytokinetic furrow and is required for cytokinesis in cultured mammalian cells (Tatsumoto et al., 1999) and *Drosophila melanogaster* (Prokopenko et al., 1999).

However, simple localization of RhoA does not necessarily reflect high RhoA activity (Pertz and Hahn, 2004). Indeed, CYK-4 (also known as MgcRacGAP), a RhoA GTPase-activating protein (GAP) that inactivates RhoA (Jantsch-Plunger et al., 2000; Minoshima et al., 2003), forms a complex with Ect2 (Somers and Saint, 2003) and likewise localizes to the furrow region (Hirose et al., 2001; Minoshima et al., 2003; Somers and Saint, 2003). The GAP activity of CYK-4 is required for cytokinesis (Hirose et al., 2001; Somers and Saint, 2003; Lee et al., 2004). Moreover, the only studies to monitor local RhoA activity during cytokinesis have led to the conclusion that RhoA activation in the furrow region either occurs only after the onset of cytokinetic apparatus specification or not at all (Yoshizaki et al., 2003, 2004), leading to the proposal that local RhoA inactivation, rather than activation, directs cytokinetic apparatus assembly (Yoshizaki et al., 2003).

Thus, whether active RhoA represents a link between microtubules and cytokinetic apparatus assembly remains unclear. In this study, we use a fluorescent reporter for RhoA activity (Benink and Bement, 2005) and four-dimensional imaging to monitor the distribution of active RhoA in echinoderm and amphibian embryonic cells. These large cells provide excellent spatial and temporal resolution, whereas the application of four-dimensional imaging ensures that spatially or temporally localized signals are not missed. Furthermore, echinoderm embryos permit a number of physical manipulations that are difficult to conduct in other systems. By exploiting these advantages, we show that microtubules specify the cleavage plane by directing the formation and spatial extent of a highly localized zone of RhoA activity.

Results

A local zone of RhoA activity during cytokinesis

If RhoA represents a link between microtubules and the cytokinetic apparatus, active RhoA should concentrate in the furrow region. To test this, fertilized eggs of *Strongylocentrotus purpuratus* (purple urchins) or *Strongylocentrotus droebachiensis* (green urchins) were microinjected with mRNA encoding eGFP fused to the Rho GTPase–binding domain (rGBD) of rhotekin (eGFP-rGBD). The rhotekin fragment binds specifically to RhoA-GTP (i.e., active RhoA) in bio-chemical pull-down assays, and eGFP-rGBD is a faithful reporter of local RhoA activity in living *X. laevis* oocytes (Benink and Bement, 2005).

Urchin embryos injected with mRNA encoding eGFP-rGBD showed sufficient expression to allow four-dimensional imaging by the two-to-four-cell stage. Four-dimensional image series showed that eGFP-rGBD consistently concentrated at the equator of purple (Fig. 1, A and B, and Video 1) and green (Fig. 1 C and Video 2, available at http://www.jcb.org/cgi/content/full/jcb.200501131/DC1) urchin blastomeres in narrow zones, coinciding precisely with the sites of furrow formation (Fig. 1, A–C). The zones moved inward in concert with ingressing cleavage furrows and disappeared after the completion of cleavage. Before anaphase, RhoA activity was apparent at a lower level throughout the cortex. This ubiquitous activity, which was more prominent in green than in purple urchins (Fig. 1 C), disappeared abruptly at the onset of anaphase before the emergence of the equatorial RhoA zone.

To confirm that eGFP-rGBD specifically labels active RhoA, we injected C3 exotransferase, a specific inhibitor of RhoA in vertebrates and echinoderms (Kishi et al., 1993), into one blastomere of two-cell embryos that were previously injected with eGFP-rGBD. C3-injected cells failed to cleave and likewise failed to concentrate eGFP-rGBD at either the cell cortex or the equator (Fig. S1, available at http://www.jcb.org/cgi/content/full/jcb.200501131/DC1). Furthermore, eGFP alone failed to concentrate at the cortex or cleavage furrow (Fig. S1).
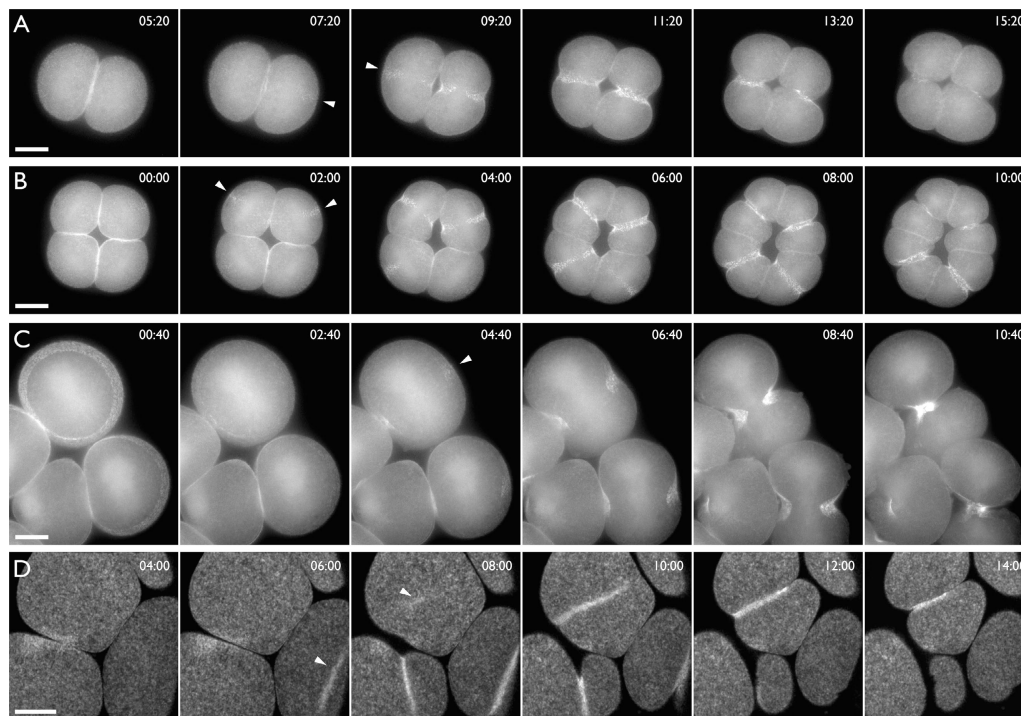

Figure 1. **A zone of RhoA activity in echinoderm and amphibian cytokinesis.** (A) Surface view of four-cell purple urchin embryo; projection of 18 1-μm sections. eGFP-rGBD begins to accumulate immediately before furrowing (arrowheads), brightens, and disappears once furrows are complete. (B) Surface view of eight-cell purple urchin embryo; projection of 18 1-μm sections. eGFP-rGBD accumulates before the furrow appears (arrowheads) at the site of the future furrow. (C) Sectional view through eight-cell green urchin embryo; projection of 16 1-μm sections. Before cleavage (00:00), eGFP-rGBD reveals uniform, cortical RhoA activity, which disappears (02:40) before localized activation of RhoA in the equator (arrowhead, 04:40), where the furrow will develop (06:40). (D) Surface view of *X. laevis* embryo; projection of 12 sections. eGFP-rGBD appears in narrow stripes (arrowheads) that presage furrow formation. See online supplemental material for Videos corresponding to B–D (Videos 1–3, respectively, available at http://www.jcb.org/cgi/content/full/jcb.200501131/DC1). Times are given in minutes:seconds after filming began. Bars, 25 μm.

To explore the generality of RhoA activation in cytokinesis, eGFP-rGBD was microinjected into embryos of two additional echinoderms—sand dollars and starfish—and the vertebrate *X. laevis*. Four-dimensional imaging confirmed that in these organisms, RhoA activation at the equator presaged cytokinesis (Fig. 1 D; Video 3; and Fig. S2, A and B, available at http://www.jcb.org/cgi/content/full/jcb.200501131/DC1). Local RhoA activation at the equator also preceded furrowing in the much smaller epithelial cells of the echinoderm and *X. laevis* blastulae and gastrulae (Fig. S2 C and not depicted).

Further analysis revealed additional features of the cytokinetic RhoA zones. First, the width of the RhoA zone remains nearly constant as furrowing progresses, as shown both by inspection (Fig. 2 A) and by signal intensity analysis of lines drawn along the plasma membrane at successive times during

cytokinesis (Fig. 2, E and F). Second, the width of the RhoA zone varied linearly in relation to cell diameter over a range of 5–15 μm (Fig. 2 G) in both species of urchin and frog (Fig. 2 H). Third, a comparison of the timing of eGFP-rGBD accumulation to furrowing onset revealed that the RhoA zone preceded furrowing by 1–4 min (Fig. 2, I and J).

The eGFP-rGBD probe also appeared to label the spindle (Fig. 2, A and B) and centrosomes (Fig. 2 B). To distinguish between probe-specific versus nonspecific labeling, we coinjected TRITC dextran and subtracted it from the eGFP-rGBD signal. This showed that only the cortical and centrosomal accumulation is specific to the eGFP-rGBD probe, whereas the apparent spindle signal reflected the exclusion of organelles from the spindle region and the corresponding enrichment of cytoplasm (Fig. 2, C and D).
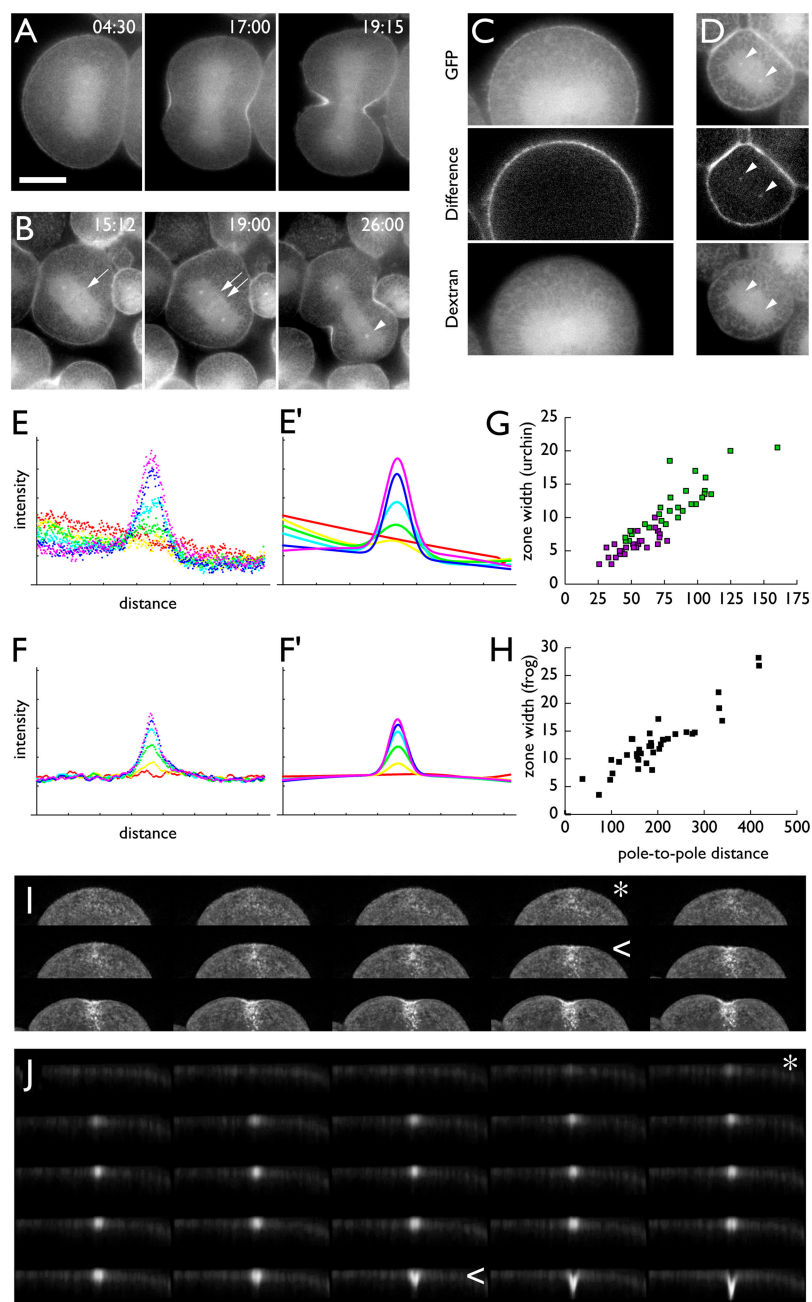

Figure 2. **Characteristics of RhoA activity zones.** (A) Single optical sections through a green urchin blastomere before, early, and late in furrowing showing zone in cross section. Bar, 25 μm. (B) Single optical sections through a blastomere from green urchin embryo showing eGFP-rGBD accumulation in spindle region. Chromosomes appear as a dark band (arrow, 15:12) that splits (arrows, 19:00) during anaphase. eGFP-rGBD highlights the centrosomes at all phases of mitosis (arrowhead, 26:00). Times are given in minutes:seconds after filming began. (C and D) Images of rGBD-eGFP (top), TRITC dextran (bottom), and difference images (middle) show that only the signal at the very cortex (C) and at the centrosome (D, arrowheads) is specific to eGFP-rGBD. Images in C are the mean of three successive frames and in D are the mean of 10 successive frames at 3-s intervals. (E and E′) eGFP-rGBD signal intensity measured along the cortex during division in green urchin. E shows raw data from single optical sections 2 min apart (from the cell shown in A), with time points ordered along the rainbow from red to violet. E′ shows curves obtained by fitting a weighted sum of a Gaussian and quadratic to the data in E. The Gaussian fits the furrow signal, whereas the quadratic fits the rest of the cortex. In this and five similar traces we performed, we note that the width of the fit Gaussian varies by 10% or less as the furrow ingresses despite the increasing curvature of the cortex. (F and F′) eGFP-rGBD signal intensity measured along the cortex during division in *X. laevis* embryo presented as in E and E′ except that time points are 20 s apart. (G) Scatter plot of RhoA activity zone width versus cell diameter in urchin embryos; purple squares come from purple urchins; green squares come from green urchins. (H) Scatter plot of RhoA activity zone width versus cell size in *X. laevis* embryos. (I) Surface view of deconvolved series showing that eGFP-rGBD concentration (asterisk) precedes furrowing (<) in purple urchin embryos; frames are 20 s apart. (J) Z image series showing that eGFP-rGBD concentration (asterisk) precedes furrowing (<) in *X. laevis* embryos.
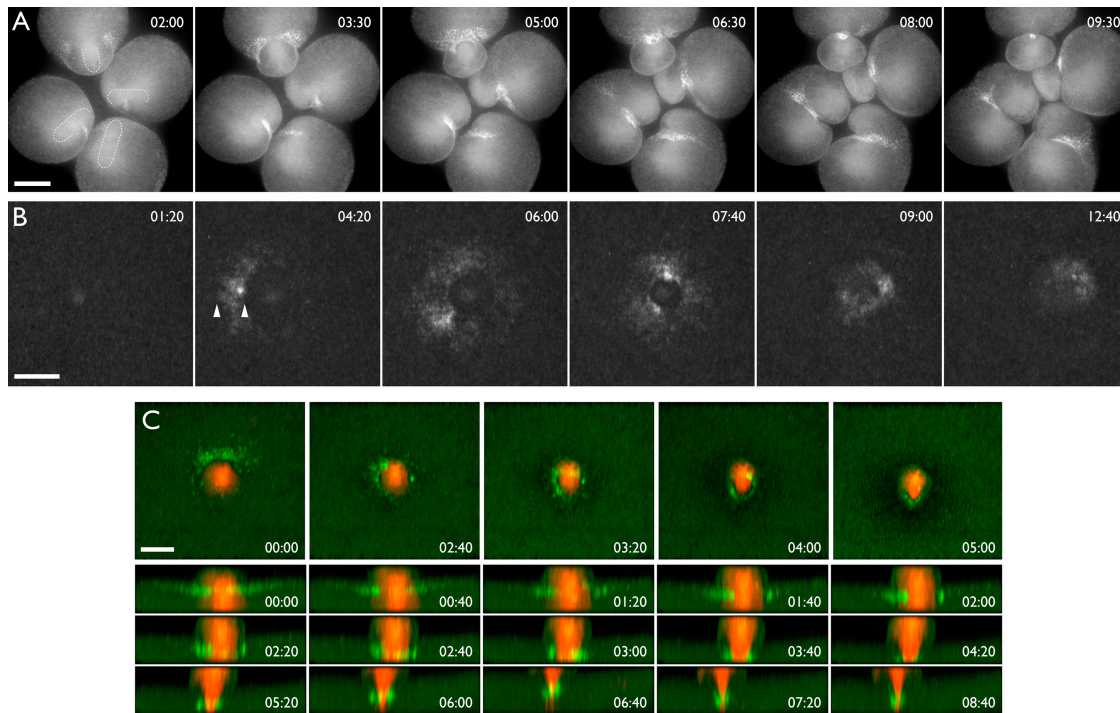
Figure 3. **RhoA zones accompany divergent forms of cytokinesis.** (A) Micromere formation in green urchin embryos. Projection of 12 1-μm sections of an eight-cell green urchin embryo. Dashed outlines in first frame show spindle position and orientation. Cell at top forms a circumferential furrow above the spindle midplane; in other cells, the asymmetric position of the spindle corresponds to asymmetric furrowing, and the region of concentrated eGFP-rGBD spreads around the circumference as furrowing proceeds. (B) Polar body formation in *X. laevis* oocytes. Projection of 13 optical sections showing that eGFP-rGBD becomes concentrated in a circular region at the animal pole and constricts inward. Arrowheads indicate edges of zone. (C) Dual-labelled images from projection of 13 optical planes showing tubulin (red) and eGFP-rGBD (green) during polar body emission. Top row shows facing view; circular region of concentrated eGFP-rGBD closes inward around microtubules of the first meiotic spindle. Bottom three rows show Z view in which eGFP-rGBD is seen to contract inward and downward in concert with the closure of the cytokinetic array, which pinches off the forming polar body. The microscope was refocused at 05:20 to allow the eGFP-rGBD ring to be followed deeper into the cytoplasm. See online supplemental material for videos corresponding to A (Video 4) and C (Video 5, available at http://www.jcb.org/cgi/content/full/jcb.200501131/DC1). All times are in minutes:seconds after filming began. Bars, 25 μm.

RhoA activity during asymmetric cytokinesis

All of the previous results depict divisions in which the cleavage furrow forms circumferentially between two equivalent mitotic asters deep in the cell. We also investigated RhoA activity in two specialized forms of cytokinesis: micromere formation in sea urchins and polar body formation in *X. laevis*. At the eight-cell stage in sea urchins, the four vegetal cells divide highly asymmetrically such that the vegetal-most daughter is ~1/30 the volume of the other. In preparation for micromere formation, the mitotic spindle develops in an eccentric position with one aster flattened against the vegetal cortex and the other deep in the cytoplasm. During micromere formation, the RhoA zone was asymmetrically positioned toward the inner edge of the blastomeres, and both formed and focused first on the side of the blastomere, where the spindle was closest, corresponding to the site of furrow initiation (Fig. 3 A and Video 4, available at http://www.jcb.org/cgi/content/full/jcb.200501131/DC1).

Polar body emission during *X. laevis* female meiosis represents the extreme of unequal cytokinesis in which the meiotic microtubule array is miniscule compared with the oocyte, and only one aster appears to interact intimately with the cortex. During polar body emission, the RhoA zone appeared as a circle at the animal pole (Fig. 3 B) and subsequently moved downward and inward in concert with the cytokinetic array that

excises the forming polar body, as revealed by the four-dimensional imaging of oocytes injected with both rhodamine tubulin and eGFP-rGBD (Fig. 3 C and Video 5, available at http://www.jcb.org/cgi/content/full/jcb.200501131/DC1). Thus, the RhoA activity zone is a feature of every variant of embryonic cytokinesis in the species we examined; in all instances, active RhoA appears in a narrow zone immediately prefiguring the site of cytokinetic furrowing.

The cytokinetic RhoA activity zone forms in the absence of actin accumulation

If the RhoA activity zone represents the link between microtubules and cytokinetic apparatus specification rather than a consequence of equatorial actin accumulation, the zone should form even under conditions in which actin cannot accumulate. We treated urchin embryos with cytochalasin D to prevent actin assembly. In purple urchin embryos, a 15–20-min treatment with cytochalasin dramatically reduced the F-actin level, and furrows failed to develop (Fig. S3, available at http://www.jcb.org/cgi/content/full/jcb.200501131/DC1). Although the cortex of these cells became obviously disrupted, forming dramatic ruffles and pleats as mitosis progressed, a RhoA zone nevertheless formed at the equator (Fig. 4 A and Video 6, available at http://www.jcb.org/cgi/content/full/jcb.200501131/DC1). Latrunculin B likewise prevented furrowing and deranged the cortex, yet did
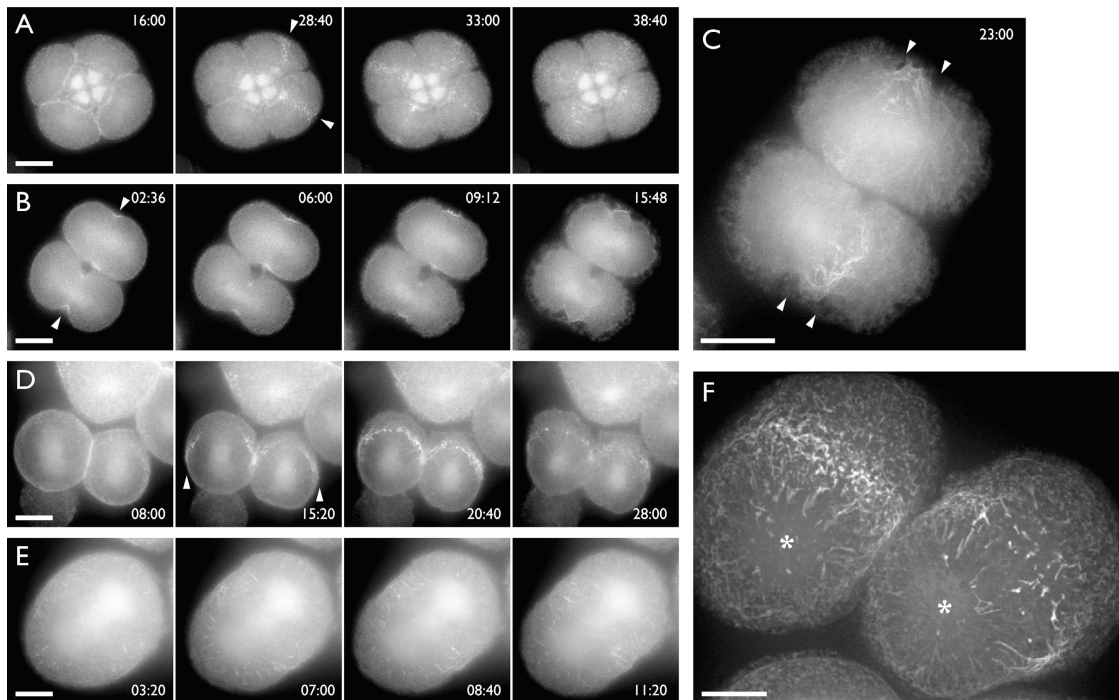
Figure 4. **RhoA activation in the equator does not depend on actin assembly.** All times in this figure are in minutes:seconds after the addition of cytochalasin D. (A) Projection of 18 1-μm sections through a 16-cell purple urchin embryo treated with 10 μM cytochalasin D during prometaphase. As the drug takes effect, cell surfaces become spiked and ruffled. Cells fail to develop a furrow but, nevertheless, form zones of RhoA activation (arrowheads, 28:40). Bright, glowing objects in other blastomeres are nuclei that accumulate eGFP probes nonspecifically (see Fig. 2, C and D). (B) Projection of four sections through a purple urchin embryo to which 10 μM cytochalasin D was added shortly before furrowing. Furrows with associated RhoA activity develop (arrowheads) and regress, but equatorial RhoA activity remains high despite furrow regression. (C) Projection of 20 sections through the near surface of the embryo shown in B; although the cortex of cytochalasin D–treated cells is wildly deranged, RhoA remains elevated in the equator (arrowheads). (D) Projection of 15 sections through a green urchin embryo to which 10 μM cytochalasin D was added at metaphase. Zones of RhoA activity (arrowheads) appear on schedule despite the absence of ingression. (E) A more extreme case than D; projection of 10 1-μm sections through one blastomere of an eight-cell green urchin embryo attempting to cleave in 12-μM cytochalasin D. Active RhoA appears on tubular extensions projecting inward from the cortex, most prominently near the equator. (F) Projection of 38 sections through an eight-cell green urchin embryo treated identically to that in E. Tubular projections point toward the spindle poles (asterisks). See online supplemental material for videos corresponding to A (Video 6) and E (Video 7, available at http://www.jcb.org/cgi/content/full/jcb.200501131/DC1). Bars, 25 μm.

not interfere with the formation of the equatorial RhoA zone (Fig. S3). When cytochalasin treatment begins shortly before cleavage, furrows may form and then regress. RhoA zones were maintained in regressing furrows (Fig. 4 B). Indeed, regressed zones persisted for 30 min or more in the presence of cytochalasin, which is more than three times as long as in control cells (Fig. 1), even when the cortex is obviously disrupted (Fig. 4 C). RhoA activity zones also formed in green urchin embryos that were treated with cytochalasin (Fig. 4 D). These results show that the equatorial activation of RhoA causally precedes F-actin accumulation.

Curiously, active RhoA was often observed to dart away from the equatorial zone inward on linear tracks that extended toward the spindle poles (unpublished data; Fig. 4 F). The inward extension of linear tracks that are rich in active RhoA could be seen in single optical sections and were particularly striking in green urchins (Fig. 4 E and Video 7, available at http://www.jcb.org/cgi/content/full/jcb.200501131/DC1), allowing quantification of the rate of inward movement (0.1–0.5 μm/s; mean = 0.2 μm/s; n = 116). These objects were not confined to the equator of cytochalasin-treated cells but were consistently brighter in the region where the furrow would have formed. Three-dimensional projections from single time points (Fig. 4 F) and brightest point projections from multiple time points (unpublished data) showed clearly that the linear tracks point toward the spindle poles. The formation of linear extensions was nocodazole sensitive (see Fig. 5 A), indicating that they are microtubule dependent.

Focusing on and maintenance of the RhoA zone depends on microtubule function

If the RhoA activity zone is the link between microtubules and cytokinetic apparatus specification, microtubule disruption should interrupt RhoA zone formation. Treatment of embryos with high concentrations of nocodazole (10–40 μM) before furrowing prevented both zone formation and furrowing but also often caused metaphase arrest, whereas treatment after the onset of furrowing usually failed to prevent either RhoA zone formation or furrow ingression (unpublished data). Therefore, we treated purple sea urchin embryos with cytochalasin to permit anaphase onset and RhoA zone formation and treated embryos with 20 μM nocodazole. In contrast to embryos exposed to cytochalasin alone, wherein the zone persisted (Fig. 4, B and C), in those treated with cytochalasin and nocodazole, the RhoA activity zones dissipated within 5–10 min of nocodazole exposure and did so in the apparent absence of the inward translocation of active RhoA on linear tracks (Fig. 5 A).
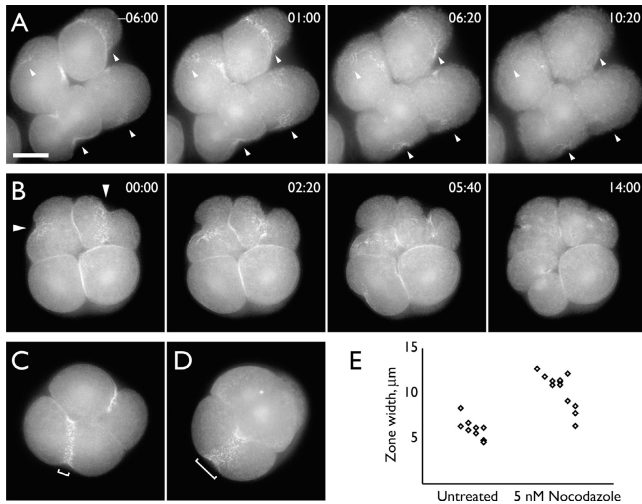
Figure 5. **Microtubule disruption disrupts RhoA zone.** (A) Projection of seven sections through a purple urchin embryo, which was first treated with 12 μM cytochalasin D immediately before furrowing, and then treated with 25 μM nocodazole at the time the furrows began to regress (00:00). Nocodazole causes rapid abolition of RhoA zones (arrowheads). Bar, 25 μm. (B) Projection of 18 sections through purple urchin embryo cultured in 5 nM nocodazole for 30 min before filming. Furrows in top two cells are associated with uneven, poorly bounded zones of RhoA activity (arrowheads, 00:00). Zones subsequently fragment, and furrows regress. (C) Projection of 18 sections through a control purple urchin embryo showing normal width and brightness of the RhoA zone during telophase. (D) Projection of 18 sections through a four-cell purple urchin embryo cultured in 5 nM nocodazole. The RhoA zone is much wider than controls (compare brackets in C and D). (E) Scatter plot showing that RhoA zones are consistently wider in embryos treated with 5 nM nocodazole. Zones were measured at the point just after ingression begins (exemplified by the lower left furrows in C and D) in four untreated and six treated embryos of equivalent developmental stage (four and eight cell) from identical experiments on two successive days. Measurements from the same embryo are aligned vertically. Control and nocodazole-treated cells are significantly different (t test: P = 10^{-6}).

As a second approach, purple urchin embryos were treated with 5 nM nocodazole in metaphase. This level of nocodazole did not cause metaphase arrest in most blastomeres but consistently resulted in abnormally broad RhoA zones and correspondingly broad furrows (Fig. 5, C–E). Four-dimensional imaging showed that such zones and furrows were highly unstable, with the RhoA zone expanding in concert with furrow broadening and regression (Fig. 5 B). In addition, RhoA activity zones were less intense than normal in cells treated with this dose of nocodazole. Similarly, green urchin embryos that were treated with 5 nM nocodazole failed to focus RhoA activity into discrete zones and failed to furrow. Thus, pharmacological disruption of microtubules disrupts both the RhoA zone and the furrow.

The RhoA activity zone responds to physical manipulations of the spindle

Micromanipulation studies have shown that changing the relationship of the spindle apparatus with respect to the cell surface results in corresponding changes in the pattern of cytokinesis in both embryos (Rappaport, 1996) and cultured cells (Alsop and Zhang, 2004). These studies show that the cytokinetic apparatus is sufficiently dynamic to reconfigure itself in response to perturbations. If the zone of RhoA activity links microtubules to cytokinetic apparatus specification, changing the relationship of the spindle to the cell surface should likewise change the pattern of RhoA activity. To explore this possibility, we deformed green urchin blastomeres, shifting the spindle relative to the cortex in various ways by using a blunt microneedle.

We first tested whether isolating the cortex from the spindle would prevent formation of the zone. We flattened cells with a microneedle (Fig. 6 A and Video 8, available at http://www.jcb.org/cgi/content/full/jcb.200501131/DC1) so as to impose the spindle on one region of the cortex while isolating the opposite edge in a flattened pouch. This manipulation resulted in a unilateral furrow and a focused RhoA zone that formed on the side of the cell closest to the displaced spindle (Rappaport and Conrad, 1963). In contrast, on the side distal to the displaced spindle, a low level of active RhoA was distributed along the entire cell edge and failed to focus into a discrete zone. No furrow formed on this side of the cell, and the RhoA-bright furrow on the spindle side divided the cell unilaterally. Thus, spindle displacement results in a corresponding change in the RhoA activity zone, which is consistent with the zone directing cytokinetic apparatus assembly.

Next, we tested whether the RhoA activity zone, once formed, could respond dynamically to a perturbation of spindle position. We had observed occasional cells in which the spindle shifted during cytokinesis and in which the RhoA zone appeared to follow (Fig. S4, available at http://www.jcb.org/cgi/content/full/jcb.200501131/DC1). To mimic this naturally occurring experiment, spindles were displaced longitudinally after RhoA zone formation and the onset of furrowing. We placed a blunt microneedle into one end of a forming daughter blastomere (without penetrating the cell), which resulted in immediate movement of the spindle away from the needle and a concomitant shift of the spindle midplane away from the furrow. After spindle displacement, the RhoA activity zone moved gradually until it was repositioned at the approximate midpoint of the displaced spindle, followed slightly later by the furrow (Fig. 6 B and Video 9, available at http://www.jcb.org/cgi/content/full/jcb.200501131/DC1). Most important, the RhoA activity zone was progressively repositioned after spindle displacement rather than simply being pulled by the spindle, as judged by the fact that zone movement occurred over the course of 3–5 min, whereas spindle movement was essentially immediate. Furthermore, cell surface irregularities in the region of the displaced spindle allowed precise tracking of the progression of RhoA zone movement relative to the cell surface (Fig. 6 B); this shows that RhoA was locally turned on in one region and turned off in another.

We then conducted the converse experiment by displacing a patch of nonequatorial cortex so that it came very close to the spindle midzone after furrowing was well underway. Within a short time, the displaced cortex exhibited intense, highly localized RhoA activity (Fig. 6 C). The activation of RhoA was not simply caused by stretching of the cell membrane, because in many similar experiments in which the needle tip did not bring the cell surface near the spindle midplane, no active RhoA was observed near the tip (Fig. 6 B). Thus, even
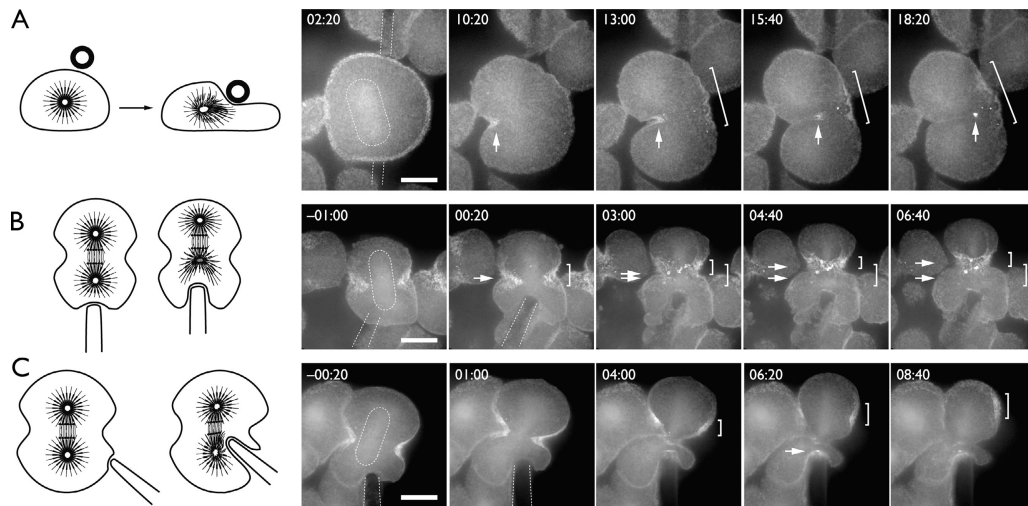
Figure 6. **Physical displacement of the cortex relative to the spindle midplane modifies the RhoA zone.** All times in this figure are in minutes:seconds relative to the physical perturbation indicated in the diagrams on the left. In each case, the dashed outlines in the first frame show the position of the spindle and the glass needle. Blastomeres from green urchin embryos at the 32–64-cell stage were used for these experiments. (A) Projection of four sections through a cell upon which the needle was pressed slightly to one side of the spindle, distending a portion of the cell into a pouch ∼10 μm thick. The side nearer the spindle initiates a tightly focused RhoA activity-rich furrow that ingresses (arrows); the far side accumulates active RhoA (brackets) but fails to focus it, and a series of shallow, unstable furrows develop and regress. (B) Projection of nine sections through a blastomere in which the spindle was displaced along the polar axis after furrow initiation. In the first frame, the blunt-ended needle is parked against one pole of the cell, slightly denting it. At 00:00, the needle was advanced by ∼15 μm (without penetrating the cell membrane), shoving the spindle so that the midplane shifts up relative to the furrow. Arrow and bracket in 00:20 mark the position immediately after the shove of the furrow and the RhoA zone, respectively, and remain the same for comparison in subsequent frames. The RhoA zone climbs higher on the cortex after the spindle midplane and is followed, in turn, by the furrow (second set of brackets and arrows in 03:00–06:40) such that the cell cleaves asymmetrically. (C) Projection of eight sections through a cell subjected to the converse of B: the cortex was displaced by a blunt needle toward the spindle midzone. In −00:20, the needle is parked slightly off center; at 00:00, the needle was advanced to bring a patch of nonequatorial cortex deep into the equatorial zone. At 06:20, needle tip shows accumulation of active RhoA (arrow). In addition, the original RhoA zone slides up the cortex (brackets in 04:00–08:40), apparently after half of the mitotic apparatus is broken by the needle. See online supplemental material for videos corresponding to A (Video 8) and B (Video 9, available at http://www.jcb.org/cgi/content/full/jcb.200501131/DC1). Bars, 25 μm.

after the onset of furrowing, the RhoA activity zone responds dynamically to changes in the relationship between the spindle apparatus and the cell surface, and the cytokinetic apparatus responds in kind to the RhoA zone. Furthermore, the nonequatorial cortex remains competent to form a RhoA activity zone even after the onset of furrowing if brought in proximity to the spindle midplane by any one of several routes (Fig. 3 A, in nearly unilateral cleavages; Fig. 6, B and C; and Fig. S4).

In normal cells, the furrow forms between two juxtaposed mitotic asters. However, recent results show that monastral spindles can induce cytokinetic furrowing (Canman et al., 2003; Alsop and Zhang, 2004). Therefore, we tested whether half spindles could induce localized RhoA activation by using a glass microneedle to bisect cells between the two asters in metaphase or anaphase. The needle was slowly lowered across the cell from one side to the other, taking special care to avoid any rupture to the cell membrane because RhoA is activated by cellular wounding (Benink and Bement, 2005). In four of five cells successfully bisected, both halves exhibited a localized elevation of RhoA activity associated with the half spindle (in the fifth case, zone formation may have occurred somewhere beyond the imaged region of the cell). Fig. 7 A depicts a cell bisected in metaphase. Starting a few minutes after cutting, RhoA activation was observed immediately adjacent to the cut spindle halves. In both halves, these zones faded minutes later without inducing a furrow. Fig. 7 B (Video 10, available at http://www.jcb.org/cgi/content/full/jcb.200501131/DC1) de-

picts a cell bisected in anaphase. Immediately after the cut, the much larger anaphase half spindles rapidly induced bright RhoA activity zones that are associated with dramatic, and in some cases multiple, furrows. Fig. 7 C shows a control cell in which the bisection separated a pouch of cytoplasm without any spindle. In all of six such cases, the spindle-containing fragment cleaved with a normal RhoA zone when the bisection took place in metaphase or before, whereas the enucleate fragment never exhibited any elevated RhoA activity.

Discussion

More than 50 yr of work has demonstrated that the geometry of the mitotic microtubule array, which interacts with the cell cortex, somehow provides the signal for cytokinetic apparatus specification in animal cells. The results of this study demonstrate that a focused region of active RhoA has all of the expected properties of the hypothetical microtubule-dependent signal for cytokinesis. First, active RhoA concentrates in a narrow zone that coincides with the furrow, and, in cases where furrowing occurs asymmetrically as a result of natural variability or physical manipulation, furrowing occurs first where active RhoA is most concentrated. Second, RhoA zone formation precedes furrowing by up to several minutes. Third, the RhoA zone is conserved in four different echinoderms and in the vertebrate *X. laevis*. Fourth, the RhoA zone not only forms during cytokinesis in blastomeres but also forms in the much smaller epithe-

Figure 7. **Each half of the mitotic apparatus can induce one zone of RhoA activation and a corresponding furrow.** Times are in minutes:seconds after the onset of filming (which began within a minute after cutting); dashed outline indicates the position of the needle. (A) Projection of eight sections through a cell bisected during metaphase. Arrowheads in the first frame indicate the centrosomes, which soon disappear from view. At approximately the time this cell would have entered anaphase, one patch of cortex near the spindle half in each cell fragment accumulates eGFP-rGBD (arrows, 06:00). (B) Projection of 10 sections through a cell cut in anaphase. The left spindle half moved away from the cut, whereas the right spindle half remained closer to the cut edge. In the left half, active RhoA immediately accumulated on the cut face near the site where the cut passed through the spindle. Within minutes, however, the spindle half in the left fragment induced a new zone (arrows in second frame), which proceeded to ingress, forming a tripartite furrow. The right half underwent unequal cleavage in association with an asymmetric RhoA zone and furrow. See Video 10 (available at http://www.jcb.org/cgi/content/full/jcb.200501131/DC1). (C) Projection of 12 sections through a cell cut (as a control for A and B) such that the entire spindle (dashed outline, 00:00) remains in one of the two fragments. Only the spindle-containing fragment exhibited elevated RhoA activity (arrow) and a cleavage furrow. Bars, 25 μm.
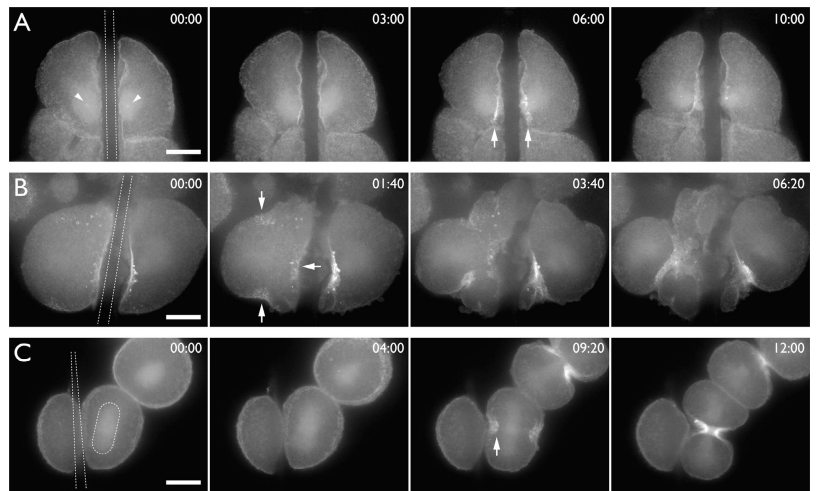
lial cells of echinoderm and *X. laevis* blastulae and gastrulae. Furthermore, the zone also forms during polar body emission, which is a highly divergent form of cytokinesis. This finding represents a particularly stringent test of functional conservation in that formation of the polar body cytokinetic apparatus is directed by microtubules of the specialized aster that abuts the cortex rather than by the spindle midzone or equatorial microtubules, which are well below the cortex (Pielak et al., 2004). Micromere formation, which is a mitotic division, occurs in the same way. Fifth, the RhoA zone forms despite disruption of the cortical actin cytoskeleton, as predicted by work showing that myosin-2, a downstream target of RhoA, accumulates at the furrow even after disruption of contractility (Straight et al., 2003). Sixth, RhoA zone formation is controlled by microtubules, as based on both pharmacological manipulation of microtubules and micromanipulation of the spindle. These findings, together with demonstrations that the inhibition of RhoA activity prevents furrowing, indicate that a zone of RhoA activity couples microtubules to cytokinetic apparatus specification.

Why, then, have previous studies of RhoA activation during cytokinesis in cultured mammalian cells led to essentially the opposite conclusion; namely, that cytokinesis is initiated by RhoA inactivation (Yoshizaki et al., 2003)? Although it is possible that mammalian cells use a fundamentally different microtubule-dependent mechanism for cytokinesis, the fact that RhoA and Ect2 inactivation prevents cytokinesis in several different cultured cell lines renders this possibility unlikely. Furthermore, RhoA itself (Yonemura et al., 2004) and its targets (Eda et al., 2001) concentrate in the furrow region. Because RhoA perturbation prevents or perturbs cytokinesis in some cell lines but not in others and produces different effects in the same cell line in different studies, it may be that different cell strains and lines have lost normal cytokinetic control mechanisms and accomplish cytokinesis by alternative means. Consistent with this possibility, the disruption of myosin-2 function can be compensated for by other mechanisms in both *Dictyostelium* (Neujahr et al., 1997) and budding yeast (Tolliday et al., 2003).

Differences in methodology could also account for the differences in findings. Because the fluorescence resonance energy transfer probe was comprised of two fluorescent protein variants fused to both RhoA and rGBD (Yoshizaki et al., 2003), it might not be recognized by the endogenous machinery that directs RhoA activation during cytokinesis. This is a possibility of particular concern given the recent demonstration that GFP-RhoA often fails to colocalize with endogenous RhoA (Yonemura et al., 2004). In addition, because samples in that study were imaged in a single focal plane at intervals of 2 min, localized and/or transient RhoA activation could have been missed.

How do microtubules direct the formation and placement of the RhoA activity zone? Studies indicate that Ect2 is responsible for RhoA activation during cytokinesis (Prokopenko et al., 1999; Tatsumoto et al., 1999), and it has been found that Ect2 binds Cyk-4 (Somers and Saint, 2003), which is a Rho family GAP that comprises part of the centralspindlin complex (Mishima et al., 2002). Because centralspindlin associates with microtubules via MKLP, a kinesin (Mishima et al., 2002; Somers and Saint, 2003), microtubules could direct the formation of the RhoA activity zone via MKLP-dependent transport.

Such a model prompts an obvious question, as does the localization of Cyk-4 to the furrow region (Hirose et al., 2001; Somers and Saint, 2003): why have RhoGAPs localized to the same region as a Rho guanine nucleotide exchange factor, where RhoA activation is required? It has previously been thought that Cyk-4 either acts late in cytokinesis to down-regulate RhoA and, thereby, permits cytokinetic apparatus disassembly (Jantsch-Plunger et al., 2000; Minoshima et al., 2003), or acts through targets other than RhoA (Somers and Saint, 2003). On the other hand, it has also been reported that Cyk-4 likely acts through RhoA (Jantsch-Plunger et al., 2000) and that disruption of its GAP activity results in a phenotype that mimics constitutively active RhoA (Lee et al., 2004).

Our results suggest a potential resolution to this paradox. First, we found that the RhoA activity zone either maintains a constant width (embryonic cytokinesis) or actually narrows

(polar body formation) while both constricting circumferentially and increasing in intensity. RhoA, like many other small GTPases, has an extraordinarily low rate of intrinsic GTPase activity (Zhang et al., 2000). Consequently, if RhoA were simply activated locally throughout active furrowing, the width of the RhoA zone should increase as its intensity increases (assuming that GTP-bound RhoA experiences some diffusional mobility). We also showed that the RhoA activity zone is rapidly remodeled after spindle displacement. Altogether, these results indicate that zone formation does not simply reflect local RhoA activation but instead reflects continual activation balanced by continual inactivation (Maddox and Oegema, 2003). Therefore, we suggest that Ect2 and Cyk-4 conspire to locally elevate the flux of RhoA through the GTPase cycle. Elevating the flux increases the availability of active RhoA without necessarily raising the standing crop and, therefore, without the risk of diffusional spread of the signal. If RhoA targets compete with Cyk-4 to bind to free GTP-bound RhoA, each of the available targets diverts some of this flux in proportion to the target concentration. Assuming RhoA targets protect bound RhoA from inactivation by RhoGAP, the major role of RhoGAP would be to inactivate the "excess" active RhoA that fails to locally interact with RhoA targets. The advantage of such a mechanism for the cell is that the ultimate targets of RhoA, such as myosin-2, can be tightly and continually focused. The consequences of failed zone focusing are revealed by the results of low concentrations of nocodazole or displacement of the spindle away from one side of the blastomere; in both cases, RhoA activity fails to focus, and the furrows that form are highly unstable. Strikingly, the disruption of Cyk-4 and p190RhoGAP, which is another RhoA GAP that localizes to the furrow region, also results in unstable and/or ectopic furrows (Su et al., 2003; Lee et al., 2004).

How, then, do microtubules of the mitotic apparatus direct the formation of the RhoA GTPase activity zone? Three general models, based on previous proposals, must be considered: (1) zone formation by delivery of the stimulus from the spindle midzone (Cao and Wang, 1996); (2) zone formation by delivery of the stimulus from overlapping, antiparallel microtubules at the equator (Devore et al., 1989; Harris and Gewalt, 1989; Somers and Saint, 2003); and (3) zone formation by delivery of the stimulus to regions of low microtubule density flanked by regions of high microtubule density (Mandato et al., 2000; Dechant and Glotzer, 2003). Ultimately, the answer to this question awaits simultaneous live cell imaging of active RhoA and microtubules as well as the development of approaches for the rapid local suppression of MKLP, Ect2, and Cyk4.

However, we suggest that the following mechanism could work for all three general models: Ect2–Cyk-4 complexes could be transported to microtubule plus ends and fall off, diffusing until they encounter another microtubule. Their transportation (when bound to microtubules) and diffusion in the cytoplasm would establish convective movement of the complex outward from astral centers. The spindle midplane would receive input from two convective sources, thereby increasing the local concentration of the Ect2–Cyk4 complex and leading to the initiation of the RhoA activity zone. Close apposition of growing microtubule ends in this region would also

act to locally muffle convection, thereby promoting rapid amplification of the zone. Then, once furrowing is underway, overlapping microtubules gathered by actomyosin-dependent ingression would sustain RhoA flux in the furrow by continually trapping the Ect2–Cyk-4 complex (Somers and Saint, 2003). Such a mechanism would explain why the zone persists in the presence of cytochalasin but is sensitive to nocodazole, whereas in the absence of actin disruption, both the zone and furrowing are impervious to nocodazole.

This mechanism also has the virtue of explaining how a RhoA activity zone might form through converging mechanisms in all of the following cases: small cells in which overlap microtubules emerge in the midplane of the cortex before furrowing; large cells in which astral microtubules only begin overlapping after the onset of furrowing; and unequally cleaving cells in which the furrow forms at the margin of a single flattened astral microtubule array. It could also explain the failure of furrowing in large cells in which a local minimum of cortical microtubule density is prevented by suppression of anaphase B (Dechant and Glotzer, 2003) because both the local suppression of convection and trapping of the Ect2–Cyk-4 complexes in a narrow region would presumably be prevented by having a broad region of microtubule overlap.

Intriguingly, results from this study exactly match the predictions of this model. That is, the width of the RhoA zone scales with the linear dimension of the cell. The angle of the wedge from the cell center to the margins of the RhoA zone is essentially constant regardless of the size of the cell in both echinoderms and *X. laevis*. Low doses of nocodazole, which limit aster growth, change this relationship, such that the zone is widened and diluted. The same result is achieved when contact between astral microtubules and the cortex is limited by physical manipulation of the blastomere. In other words, the reduction of contact between astral microtubules and the cortex by either pharmacological or physical means does not prevent RhoA activation but does prevent zone focusing and stabilization.

One of the most fascinating aspects of local RhoA activity during cytokinesis is its striking similarity to RhoA activity in *X. laevis* oocyte wound healing (Benink and Bement, 2005). That is, wounding elicits activation of RhoA in a broad region that rapidly focuses into a narrow zone around the site of plasma membrane damage and then moves inward in concert with a circular array of F-actin and myosin-2. Like the cytokinetic RhoA activity zone, the wound zone is tightly bounded and forms independently of cortical F-actin. It is also modulated by microtubules, though to a lesser degree than the cytokinetic RhoA zone (Benink and Bement, 2005). The striking similarity between the two systems supports the proposal that cytokinesis and single-cell wound healing have common evolutionary roots and that findings from the wound healing system may be extrapolated to cytokinesis (Mandato and Bement, 2001). Two features of the wound healing system are particularly noteworthy in this context. The first is the finding that the wound RhoA zone directs the local accumulation of phosphorylated (activated) myosin-2. Therefore, we suggest that the cytokinetic RhoA zone directs and maintains myosin-2 phosphorylation specifically at the furrow region, where it is needed.

The second feature of the wound healing system that may be relevant to cytokinesis is the formation of a complementary zone of Cdc42 activation that circumscribes the RhoA zone (Benink and Bement, 2005). Although we do not yet know if active Cdc42 forms a similar zone during cytokinesis, this possibility is consistent with the reported Cdc42 dependence of cytokinesis in *X. laevis* embryos (Drechsel et al., 1997) and the proposal that complementary regions of local Rho-class GTPase activation could explain many of the features of cytokinesis (Mandato et al., 2000; Yoshizaki et al., 2004). In particular, local activation of Cdc42 and/or Rac1 in regions flanking the RhoA zone could enhance furrowing by reducing contractility outside the RhoA zone. This is accomplished either by directly suppressing myosin-2 phosphorylation (Sanders et al., 1999) or by negative cross talk with RhoA itself (Benink and Bement, 2005), which is another potential mechanism for maintaining RhoA zone boundaries.

Materials and methods

Animals and embryos

Purple urchins (*S. purpuratus*) were collected intertidally and maintained in submerged cages. Green urchins (*S. droebachiensis*) were collected either by dredging or by hand and were maintained in flowing seawater tanks. Starfish (*Pisaster ochraceus*) and sand dollars (*Dendraster excentricus*) were collected by hand, and sand dollars were maintained on a layer of sand in flowing seawater tanks. *X. laevis* embryos (provided by T. Gomez, University of Wisconsin-Madison, Madison, WI) were obtained as described in Gomez et al. (2003).

All urchin egg–handling procedures were performed next to a flowing seawater table to maintain eggs and embryo cultures at 10–12°C. Urchins and sand dollars were spawned by intracoelomic injection of 0.55 M KCl. Semen was collected dry. Eggs were collected in coarse-filtered natural seawater (NSW) and suspended in 10 ml NSW in a 15-ml centrifuge tube and were fertilized by adding 1–2 ml of semen diluted 1:10,000 in NSW. After 30–90 s, eggs were pelleted by 10–12 spins in a hand centrifuge, and NSW was replaced with artificial calcium/magnesium-free seawater (CMFSW): 450 mM NaCl, 33 mM Na_2SO_4, 9 mM KCl, 2.5 mM $NaHCO_3$, 10 mM Tris, and 1 mM EDTA, adjusted to pH 7.8–8.0. Eggs in CMFSW were settled twice more in a hand centrifuge, replacing CMFSW with fresh CMFSW within 2–3 min. Purple urchin vitellines were removed by passing eggs once through 73-μm Nitex mesh in CMFSW; green urchin vitellines were dissolved with gentle pipetting. Eggs were allowed to settle by gravity alone and were resuspended in several changes of NSW. Fertilized eggs were never allowed to remain in CMFSW for >12 min. Sand dollar egg vitellines were stripped by sieving the fertilized eggs 10–20 min after fertilization through 110-μm Nitex mesh. Starfish oocytes were obtained after the dissection of a single ray and removal of the ovary. After injection, starfish oocytes were matured by the addition of 10 μM 1-methyladenine and were fertilized after germinal vesicle breakdown by the addition of dilute sperm.

Reagents and microinjections

Constructs were generated as previously described (Benink and Bement, 2005). mRNA encoding eGFP-rGBD (from mouse rhotekin) or eGFP alone was transcribed in vitro using the mMessage mMachine kit (Ambion) from eGFP or eGFP-rGBD in pCS2 and was stored at −80°C until use. C3 exotransferase (Cytoskeleton, Inc.) was also stored at −80°C until use. Cytochalasin D (Sigma-Aldrich) was freshly dissolved in NSW to twice the intended concentration and kept on ice until use. To ensure rapid mixing of the drug, half the seawater droplet in which the embryos were cultured during imaging was removed and replaced with cytochalasin-containing seawater. Nocodazole (Sigma-Aldrich) was prepared similarly at double the desired final concentration from a stock solution of 5 mM in DMSO and added to embryos in the same manner. Latrunculin B (Sigma-Aldrich) was dissolved in NSW to 12 μM from a 15-mM stock in DMSO, and eggs were added to this solution and mixed rapidly before imaging. Rhodamine tubulin (Cytoskeleton, Inc.) was diluted in PBS before use to a final concentration of 2 mg/ml, and then centrifuged at 100,000 g for 30 min to clear aggregates.

For echinoderm microinjections, embryos were cultured in watch glasses licked recently by G. von Dassow and were transferred by mouth pipette (also spit rinsed) into NSW in the wells of glass-bottomed dishes (MatTek). Needles were pulled from silanized glass tubes, broken to a tip opening <5 μm wide, and mounted at ∼45°C on a manual micromanipulator next to a stereomicroscope (model Falcon XR8; Choad Instruments). Embryos were maintained below 12°C during microinjection with a thermoelectric cooling stage (Dagan). Needles were backfilled with the desired injectate and coupled to a pneumatic microinjector (model Picospritzer III; Parker-Hannifin) calibrated to deliver 2–3% of the egg volume at one pulse. Most injected eggs routinely survived injections of this volume, developing into regular blastulas and gastrulas on a relatively normal schedule whether injected with mRNA for various probes, fluorescent dextrans, labeled tubulin, or other probes.

In some cases, purple urchin eggs were dejellied, settled onto poly lysine or protamine sulfate-coated glass in a drop of seawater containing 1 mM 3-aminotriazole to slow hardening of the vitelline, and injected immediately after the addition of dilute sperm. In this approach, embryos retained their hyaline layer, which helped keep embryonic blastomeres together. Otherwise, early embryos tended not to maintain the typical arrangement of cells as they cleaved. The presence or absence of the hyaline layer made no difference in the sensitivity of embryos to cytochalasin D, latrunculin B, or nocodazole. Injected embryos were returned to the sea table for culture until they began to express the probe.

For frog embryos, microneedles were broken to a tip size of 10–20 μm, mounted on a picoinjector (model PLI-100; Medical Systems, Inc.), suction filled, and calibrated by injecting them into an oil droplet. Embryos were injected into one blastomere of two-to-four-cell stages with a 5-nl vol of eGFP-rGBD at 1 mg/ml.

Microscopy

Echinoderm embryos were imaged in the same dishes used for injection and were inserted into a thermoelectric cooling stage insert (Dagan) to maintain them at 10–12°C. All imaging of urchin, sand dollar, and starfish embryos was conducted using a PlanApo 60× water immersion objective (1.2 NA; Nikon) mounted on an inverted microscope (model TE2000; Nikon) coupled to a spinning disk unit (model CARV; Atto Biosciences), and images were collected on a camera (model ORCA ER; Hamamatsu). The four-dimensional image series used shuttered illumination to protect embryos from light damage. Microscope automation and image analysis were performed using MetaMorph v. 6x. Selected images were subjected to deconvolution by using either AutoDeblur v. 10 (AutoQuant Imaging, Inc.) or Volocity v. 3 (Improvision). Images of echinoderm embryos were processed as follows: cropped and maximum projected using MetaMorph, contrast stretched, gamma adjusted, converted to eight-bit depth using ImageJ, and compressed using QuickTime. The rationale for contrast and gamma adjustment was as follows: because, for the most part, our probe is fluorescent throughout the cytoplasm and the spinning disk experiences some cross talk from adjacent pinholes, each image includes an unavoidable "glow" from far-from-focused regions of the embryo (this is not a problem with tightly localized probes or with thinner specimens such as isolated blastomeres). This glow is much dimmer than the in-focus regions, and, therefore, appears as a lower peak in the histogram of image intensities. Rather than trim off the entire background peak, we set the black level slightly below the modal value for the lower peak and used a mild gamma of 1.2 while setting the white level such that 0.01–0.1% of pixels in the cell of interest were saturated. Frog embryos were mounted in a ring of high vacuum grease on a slide, covered with a coverslip 3–18 h after microinjection, and imaged on a microscope (model Axiovert; Carl Zeiss MicroImaging, Inc.) using a confocal system (model 1024; Bio-Rad Laboratories). Four-dimensional image series were processed using Volocity and converted to QuickTime videos as described in the previous paragraph.

Micromanipulations

Micromanipulations were conducted using a hanging joystick oil hydraulic micromanipulator (model MO-202D; Narishige). Glass needles were hand pulled to yield a long filament and were broken by striking if a blunt probe was required. Sharp edges were removed by briefly bringing the probe near an alcohol flame.

Online supplemental material

Fig. S1 shows the specificity of the eGFP-rGBD probe. Fig. S2 illustrates RhoA activity zones in two additional echinoderm species and in embryonic epithelial cells. Fig. S3 shows the effect of 12-μM cytochalasin D treatment on the F-actin content of the embryo and also shows that latruncu-

lin B (like cytochalasin) prevents furrowing without interfering with RhoA zone formation. Fig. S4 supplements Fig. 6 B by showing that RhoA activation in the furrow follows the spindle midplane in naturally occurring cases in which the spindle moves relative to the cleavage furrow. Videos 1 and 2 show the accumulation of eGFP-rGBD in the urchin furrow and correspond to Fig. 1 (B and C, respectively). Video 3 shows the accumulation of eGFP-rGBD in the *X. laevis* furrow and corresponds to Fig. 1 D. Video 4 shows RhoA activity during unequal cleavage (micromere formation) in the urchin embryo and corresponds to Fig. 3 A. Video 5 shows RhoA activity during polar body emission in *X. laevis* and corresponds to Fig. 3 C. Video 6 shows that the RhoA zone forms in the presence of cytochalasin D and corresponds to Fig. 4 A. Video 7 shows RhoA activity after extreme disruption of the cortex by cytochalasin D and corresponds to Fig. 4 E. Video 8 shows that isolation of the cortex from the spindle prevents focusing of the RhoA activity zone and corresponds to Fig. 6 A. Video 9 shows that the RhoA activity zone moves after displacement of the spindle and corresponds to Fig. 6 B. Video 10 shows that half spindles induce RhoA activation and corresponds to Fig. 7 B. Online supplemental material is available at http://www.jcb.org/cgi/content/full/jcb.200501131/DC1.

References

Abraham, I., M. Marcus, F. Cabral, and M.M. Gottesman. 1983. Mutations in α- and β-tubulin affect spindle formation in Chinese hamster ovary cells. *J. Cell Biol.* 97:1055–1061.

Alsop, G.B., and D. Zhang. 2004. Microtubules continuously dictate distribution of actin filaments and positioning of cell cleavage in grasshopper spermatocytes. *J. Cell Sci.* 117:1591–1602.

Benink, H.A., and W.M. Bement. 2005. Concentric zones of active RhoA and Cdc42 around single cell wounds. *J. Cell Biol.* 168:429–439.

Canman, J.C., L.A. Cameron, P.S. Maddox, A. Straight, J.S. Tirnauer, T.J. Mitchison, G. Fang, T.M. Kapoor, and E.D. Salmon. 2003. Determining the position of the cell division plane. *Nature.* 424:1074–1078.

Cao, L.G., and Y.L. Wang. 1996. Signals from the spindle midzone are required for the stimulation of cytokinesis in cultured epithelial cells. *Mol. Biol. Cell.* 7:225–232.

Dechant, R., and M. Glotzer. 2003. Centrosome separation and central spindle assembly act in redundant pathways that regulate microtubule density and trigger cleavage furrow formation. *Dev. Cell.* 4:333–344.

Devore, J.J., G.W. Conrad, and R. Rappaport. 1989. A model for astral stimulation of cytokinesis in animal cells. *J. Cell Biol.* 109:2225–2232.

Drechsel, D.N., A.A. Hyman, A. Hall, and M. Glotzer. 1997. A requirement for Rho and Cdc42 during cytokinesis in *Xenopu*s embryos. *Curr. Biol.* 7:12–23.

Eda, M., S. Yonemura, T. Kato, N. Watanabe, T. Ishizaki, P. Madaule, and S. Narumiya. 2001. Rho-dependent transfer of Citron-kinase to the cleavage furrow of dividing cells. *J. Cell Sci.* 114:3273–3284.

Gomez, T.M., D. Harrigan, J. Henley, and E. Robles. 2003. Working with *Xenopus* spinal neurons in live cell culture. *Methods Cell Biol.* 71:129–156.

Hamaguchi, Y. 1975. Microinjection of colchicine into sea urchin eggs. *Dev. Growth Differ.* 17:111–117.

Harris, A.K., and S.L. Gewalt. 1989. Simulation testing of mechanisms for inducing the formation of the contractile ring in cytokinesis. *J. Cell Biol.* 109:2215–2223.

Hiramoto, Y. 1956. Cell division without mitotic apparatus in sea urchin eggs. *Exp. Cell Res.* 11:630–636.

Hirose, K., T. Kawashima, I. Iwamoto, T. Nosaka, and T. Kitamura. 2001. MgcRacGAP is involved in cytokinesis through associating with mitotic spindle and midbody. *J. Biol. Chem.* 276:5821–5828.

Jantsch-Plunger, V., P. Gonczy, A. Romano, H. Schnabel, D. Hamill, R. Schnabel, A.A. Hyman, and M. Glotzer. 2000. CYK-4: a Rho family GTPase activating protein (GAP) required for central spindle formation and cytokinesis. *J. Cell Biol.* 149:1391–1404.

Kishi, K., T. Sasaki, S. Kuroda, T. Itoh, and Y. Takai. 1993. Regulation of cytoplasmic division of *Xenopus* embryo by rho p21 and its inhibitory GDP/GTP exchange protein (rho GDI). *J. Cell Biol.* 120:1187–1195.

Lee, J.S., K. Kamijo, N. Ohara, T. Kitamura, and T. Miki. 2004. MgcRacGAP

regulates cortical activity through RhoA during cytokinesis. *Exp. Cell Res.* 293:275–282.

Mabuchi, I., Y. Hamaguchi, H. Fujimoto, N. Morii, M. Mishima, and S. Narumiya. 1993. A rho-like protein is involved in the organisation of the contractile ring in dividing sand dollar eggs. *Zygote.* 1:325–331.

Maddox, A.S., and K. Oegema. 2003. Closing the GAP: a role for RhoA GAP in cytokinesis. *Mol. Cell.* 11:846–848.

Mandato, C.A., and W.M. Bement. 2001. Contraction and polymerization cooperate to assemble and close actomyosin rings around *Xenopus* oocyte wounds. *J. Cell Biol.* 154:785–797.

Mandato, C.A., H.A. Benink, and W.M. Bement. 2000. Microtubule-actomyosin interactions in cortical flow and cytokinesis. *Cell Motil. Cytoskeleton.* 45:87–92.

Minoshima, Y., T. Kawashima, K. Hirose, Y. Tonozuka, A. Kawajiri, Y.C. Bao, X. Deng, M. Tatsuka, S. Narumiya, W.S. May Jr., et al. 2003. Phosphorylation by aurora B converts MgcRacGAP to a RhoGAP during cytokinesis. *Dev. Cell.* 4:549–560.

Mishima, M., S. Kaitna, and M. Glotzer. 2002. Central spindle assembly and cytokinesis require a kinesin-like protein/RhoGAP complex with microtubule bundling activity. *Dev. Cell.* 2:41–54.

Neujahr, R., C. Heizer, and G. Gerisch. 1997. Myosin II-independent processes in mitotic cells of *Dictyostelium discoideum*: redistribution of the nuclei, re-arrangement of the actin system and formation of the cleavage furrow. *J. Cell Sci.* 110:123–137.

Pertz, O., and K.M. Hahn. 2004. Designing biosensors for Rho family proteins–deciphering the dynamics of Rho family GTPase activation in living cells. *J. Cell Sci.* 117:1313–1318.

Pielak, R.M., V.A. Gaysinskaya, and W.D. Cohen. 2004. Formation and function of the polar body contractile ring in *Spisula*. *Dev. Biol.* 269:421–432.

Prokopenko, S.N., A. Brumby, L. O'Keefe, L. Prior, Y. He, R. Saint, and H.J. Bellen. 1999. A putative exchange factor for Rho1 GTPase is required for initiation of cytokinesis in *Drosophila*. *Genes Dev.* 13:2301–2314.

Rappaport, R. 1961. Experiments concerning the cleavage stimulus in sand dollar eggs. *J. Exp. Zool.* 148:81–91.

Rappaport, R. 1996. Cytokinesis in Animal Cells. Cambridge University Press, New York. 386 pp.

Rappaport, R., and G.W. Conrad. 1963. An experimental analysis of unilateral cleavage in invertebrate eggs. *J. Exp. Zool.* 153:99–112.

Sanders, L.C., F. Matsumura, G.M. Bokoch, and P. de Lanerolle. 1999. Inhibition of myosin light chain kinase by p21-activated kinase. *Science.* 283:2083–2085.

Somers, W.G., and R. Saint. 2003. A RhoGEF and Rho family GTPase-activating protein complex links the contractile ring to cortical microtubules at the onset of cytokinesis. *Dev. Cell.* 4:29–39.

Straight, A.F., A. Cheung, J. Limouze, I. Chen, N.J. Westwood, J.R. Sellers, and T.J. Mitchison. 2003. Dissecting temporal and spatial control of cytokinesis with a myosin II inhibitor. *Science.* 299:1743–1747.

Su, L., J.M. Agati, and S.J. Parsons. 2003. p190RhoGAP is cell cycle regulated and affects cytokinesis. *J. Cell Biol.* 163:571–582.

Takaishi, K., T. Sasaki, T. Kameyama, S. Tsukita, S. Tsukita, and Y. Takai. 1995. Translocation of activated Rho from the cytoplasm to membrane ruffling area, cell-cell adhesion sites and cleavage furrows. *Oncogene.* 11:39–48.

Tatsumoto, T., X. Xie, R. Blumenthal, I. Okamoto, and T. Miki. 1999. Human ECT2 is an exchange factor for Rho GTPases, phosphorylated in G2/M phases, and involved in cytokinesis. *J. Cell Biol.* 147:921–928.

Tolliday, N., M. Pitcher, and R. Li. 2003. Direct evidence for a critical role of myosin II in budding yeast cytokinesis and the evolvability of new cytokinetic mechanisms in the absence of myosin II. *Mol. Biol. Cell.* 14:798–809.

Yonemura, S., K. Hirao-Minakuchi, and Y. Nishimura. 2004. Rho localization in cells and tissues. *Exp. Cell Res.* 295:300–314.

Yoshizaki, H., Y. Ohba, K. Kurokawa, R.E. Itoh, T. Nakamura, N. Mochizuki, K. Nagashima, and M. Matsuda. 2003. Activity of Rho-family GTPases during cell division as visualized with FRET-based probes. *J. Cell Biol.* 162:223–232.

Yoshizaki, H., Y. Ohba, M.C. Parrini, N.G. Dulyaninova, A.R. Bresnick, N. Mochizuki, and M. Matsuda. 2004. Cell type-specific regulation of RhoA activity during cytokinesis. *J. Biol. Chem.* 279:44756–44762.

Zhang, B., Y. Zhang, Z. Wang, and Y. Zheng. 2000. The role of Mg^{2+} cofactor in the guanine nucleotide exchange and GTP hydrolysis reactions of Rho family GTP-binding proteins. *J. Biol. Chem.* 275:25299–25307.